KSCE Journal of Civil Engineering (2016) 20(2):803-812
DOI 10.1007/s12205-015-0461-6

Structural Engineering
pISSN 1226-7988, eISSN 1976-3808
www.springer.com/12205

A Stereovision-based Crack Width Detection Approach for Concrete Surface Assessment

Baohua Shan*, Shijie Zheng, and Jinping Ou*****

Received August 12, 2014/Revised December 28, 2014/Accepted March 15, 2015/Published Online April 20, 2015

Abstract

To quantitatively evaluate crack width of concrete structures surface, this paper presents a stereovision-based crack width detection method. Compared with the traditional visual inspection with single camera, this approach uses a pair of cameras to capture cracks images for recovering 3D coordinates of crack edge, and does not needs scale attached to concrete surface for converting measurement unit. A novel Canny-Zernike combination algorithm is utilized to obtain the image coordinates of crack edge in the left crack image, this combination algorithm can achieve 0.02 subpixel precision. The 3D coordinates of crack edge are acquired by projecting crack edge curve on concrete surface where cracks are located. The crack width is assessed by the minimum distance between two sides of crack edge. The detection tests are conducted on three concrete beams destroyed in static test, and the crack width of two inspection zones on each beam is acquired. Experimental results indicate that the stereovision-based crack width detection approach can accurately measure the crack width compared with the crack width gauge or the vernier calliper. This verifies the proposed method is applicable and useful for assessing the crack width of concrete surface.

Keywords: *crack width, detection, stereovision, three-dimensional (3D), concrete surface*

1. Introduction

The type, number, width and length of cracks on structural surface directly reflect the earliest degradation levels and carrying capacity of concrete structures. Therefore, accurately evaluating cracks is the most important step during inspection, diagnosis, and life prediction for the safety of concrete structures. At present, several methods for detecting cracks on concrete structures are available, such as visual inspection, ultrasonic, fiber optics and photogrammetry. Visual inspection is manually carried out by experienced inspectors using a crack scale and a loupe. It is time-consuming, tedious, subjective and highly quantitative approach. The ultrasonic method can detect the depth and width of cracks, but it needs coupling agent to measure cracks, which leads to inconvenient operation in practice (McCann *et al*., 2001). The fiber optics approach needs to bury fiber optics sensors into structures or attach them to structural surface in advance, and measures the crack width and location by utilizing the change of light intensity. However, laying fiber optics sensors on structures also creates the complexity of measurement (Zhang *et al*., 2007).

Compared with previously mentioned inspection methods, the photogrammetry approach has the merits of non-contact, rapidity of implementation and convenience (Li *et al.*, 2010; Kai *et al*., 2007). In the past twenty years, the image-based crack detection technique has developed quickly, and has been widely applied in civil structures, such as bridges, tunnels, pavements and hydraulic structures. Dare et al (2003) proposed a crack detection method based on semi-automatic feature extraction, and used bilinear interpolation of pixel values to calculate crack width. However, the measurement unit of this method was pixels. Li *et al.* (2009) introduced the gray system theory to inspect the pavement crack and proposed an improved image preprocessing and segmentation algorithm based on gray system theory. Yamaguchi and Hashimoto (2010) presented a percolation-based crack detection method to reduce the computation time, in which the crack width measurement was performed during the morphological thinning operation. However, those approaches require a crack-scale attachment to estimate the crack width in millimeters and prior calibration. Jahanshahi and Masri (2013) utilized the depth perception to quantify crack thickness. This method was ideal for incorporation with autonomous or semi-autonomous mobile inspection.

As can be seen from the above, there are few studies regarding

*Associate Professor, School of Civil Engineering, Harbin Institute of Technology, Harbin 150090, China (Corresponding Author, E-mail: shanbaohua@hit.edu.cn)
**Assistant Professor, School of Civil Engineering, Harbin Institute of Technology, Harbin 150090, China (E-mail: zhengshijie@hit.edu.cn)
***Professor, Academician of Chinese Academy of Engineering, School of Civil Engineering, Harbin Institute of Technology, Harbin 150090, China (E-mail: Oujinping@hit.edu.cn)

the vision-based quantification of crack width. In addition, most of the previous studies use one camera to capture crack image. This requires the lens of CCD camera to be perpendicular to the crack surface during detection. When the inspection angle or the distance between CCD camera and the object change, errors occur due to the perpendicular requirement of lens. In that case, the CCD camera must be calibrated again with a scale attached, which converts the quantified crack width from pixels to millimeters.

To solve the above problems, a stereovision-based crack width detection method is proposed in this study. The equation of structural surface where cracks are located is established by extracting any three feature points which do not line up, with SIFT algorithm. 3D coordinates of crack edge are recovered by projecting crack edge curve onto space plane where cracks are located, and crack width of concrete surface is assessed by the minimum distance between two sides of crack edge. Since no scale needs to stick to concrete surface for unit conversion, experimental preparation is simple, easy to carry out, with no negative effects on structures.

2. Stereovision-based Crack Width Detection Approach

Based on the parallax theory, stereovision approach accomplishes 3D measurement. In usual case, there exist no requirements for two cameras' positions (Longuet-Higgins, 1981). As shown in Fig. 1, assuming that the left camera coordinate system is located on the original point of the world coordinate system and does not rotate, $O_l-X_lY_l$ is the corresponding image coordinate system of left camera; $o_r-x_ry_rz_r$ is the right camera coordinate system, $O_r-X_rY_r$ is the corresponding image coordinate system of right camera.

Supposing that the matching relationship of the corresponding points on the left and right images has been already known, the 3D coordinates of feature point in the global coordinate system can be obtained according to the geometry constraint of binocular sensors, and the equation is expressed as follows:

$$\begin{cases} x = zX_l/f_l \\ y = zY_l/f_l \\ z = \dfrac{f_l(f_r t_x - X_r t_z)}{X_r(r_7X_l + r_8Y_l + f_l r_9) - f_r(r_1X_l + r_2Y_l + f_l r_3)} \end{cases} \quad (1)$$

where f_l and f_r are the effective focal lengths of the left and right camera, respectively. As can be seen from Eq. (1), if the effective focal length f_l, f_r and the image coordinates (X_l, Y_l), (X_r, Y_r) of feature point in the left and right image coordinate system are all known, the 3D coordinates (x, y, z) of feature point in the left camera coordinate system can be calculated provided that the rotation matrix $R = \begin{bmatrix} r_1 & r_2 & r_3 \\ r_4 & r_5 & r_6 \\ r_7 & r_8 & r_9 \end{bmatrix}$, and translation matrix can be solved, therein the extrinsic parameters $[R\ T]$ can be acquired by Zhang's calibration algorithm based on 2D planar pattern (Zhang, 2000).

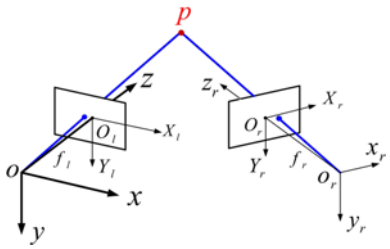

Fig. 1. Mathematical Model of Stereovision Measurement.

Currently, there exist the horizontal scale method and the average width method for computing crack width. Therein, the horizontal scale method mainly applies to the vertical crack in image. It calculates the coordinate difference of the left and right edge on each line to obtain crack width. Because this approach doesn't consider crack slope, it brings greater errors during measurement. The average width method needs to compute the crack area and length after obtaining the binary crack image, the ration between area and length is the average width. However, only the maximum crack width is applied to assess structural damage condition under normal conditions. Consequently, this study calculates the minimum distance to evaluate crack width of concrete surface.

Based on the two sides of crack edge, the minimum distance computes the shortest distance from each point on one side to any point on another side by using Eq. (2) as follows. This distance is the crack width of that point on one side.

$$w_i = \min(\sqrt{(x_i - x_j)^2 + (y_i - y_j)^2 + (z_i - z_j)^2}) \quad (2)$$

$$j = 1, 2, 3, \ldots\ldots n$$

To acquire 3D coordinates of crack edge, the crack image captured by the left camera is projected on the space plane where structural surface is located in this study. As shown in Fig. 2, the world coordinate system $o-xyz$ is established on the optical center of the left camera, coinciding with the left camera coordinate system. Both image coordinate systems $O_l-X_lY_l$ and O_o-

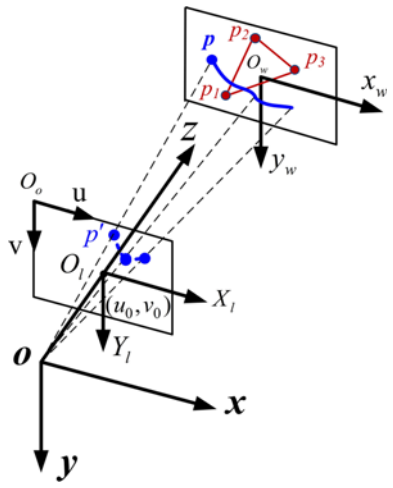

Fig. 2. Space Projection of Crack Edge

uv are located on the normalized virtual imaging plane where z is equal to 1. The coordinate system $o_w - x_w y_w$ is the space plane where structural surface is positioned.

As shown in Fig. 2, a point $p(x, y, z)$ is located at the edge of surface crack, and the corresponding point p' is projected on the normalized virtual imaging plane. The pixel coordinates of point p' in the image coordinate system $O_o - uv$ (units: pixel) is (u_l, v_l), and the 3D coordinates of point p' on the normalized virtual imaging plane are $(X_l, Y_l, 1)$, where (X_l, Y_l) is the physical coordinate of point p' in the image coordinate system $O_l - X_l Y_l$ (units: mm). The transformation relation between the pixel image coordinate systems $O_o - uv$ and the physical image coordinate system $O_l - X_l Y_l$ is given as follows:

$$\begin{bmatrix} u_l \\ v_l \\ 1 \end{bmatrix} = \begin{bmatrix} f_x & 0 & u_o \\ 0 & f_y & v_o \\ 0 & 0 & 1 \end{bmatrix} \begin{bmatrix} X_l \\ Y_l \\ 1 \end{bmatrix} \tag{3}$$

where is the known intrinsic parameter of the left camera, f_x, f_y are the normalized focal length on u, v axis, respectively, (u_0, v_0) is the coordinate of principal point in the image coordinate system $O_o - uv$.

From Eq. (3), the 3D coordinates $(X_l, Y_l, 1)$ of point p' on the normalized virtual imaging plane can be obtained. Accordingly, the 3D coordinates of point $P(x, y, z)$ on the crack edge can be achieved by calculating the intersection point between the straight line op' and the structural plane where the crack is located. Therefore, the key issue of this study is how to recover the equation of structural surface where the crack is positioned in the world coordinate system.

In this study, the equation of structural surface where the crack is located, is established by any three points, $p_1(x_3, y_3, z_3)$, and $p_2(x_3, y_3, z_3)$ which do not line up. It should be noted that any three points p_1, p_2, p_3 on structural surface are not located on the crack. Thus, the normal vector of the structural surface where the crack is positioned is defined as follows:

$$\begin{cases} \overrightarrow{p_1 p_2} = (x_2 - x_1, y_2 - y_1, z_2 - z_1) \\ \overrightarrow{p_1 p_3} = (x_3 - x_1, y_3 - y_1, z_3 - z_1) \\ \vec{n} = \overrightarrow{p_1 p_2} \times \overrightarrow{p_1 p_3} \end{cases} \tag{4}$$

where the normal vector $\vec{n}$ can be obtained by Eq. (4). The unique structural plane equation is expressed as follows:

$$p(x, y, z) - p_1(x_1, y_1, z_1) \cdot \vec{n} = 0 \tag{5}$$

In this study, the 3D coordinates of p_1, p_2, p_3 can be calculated by Eq. (1). From Eqs. (4) and (5), the equation of structural surface where the crack is located is finally achieved.

3. Image Processing

It is important to note that any three points p_1, p_2, p_3 on structural plane are feature points in the crack image captured by the left and right camera, respectively. According to the parallax of the same feature point in left and right images, this paper employs the binocular stereovision approach to reconstruct 3D coordinate of the feature point through feature extraction and matching. Therefore, the main issue of crack width measurement is how to identify the same feature point in the left and right images.

3.1 Extraction and Matching of Feature Points

At present, many feature points extraction methods are available, such as Harris corner detection algorithm (Bellavia *et al.*, 2011), SUSAN corner extraction algorithm (Smith and Brady, 1997), and SIFT (Scale Invariant Feature Transform) extraction algorithm (Lowe, 1999 and 2004). Due to the robustness of SIFT algorithm to distortion, change of measured point, noise, change of light intensity, etc., SIFT algorithm is chosen to extract feature points on the left and right crack image in this study.

Based on the scale selection of image feature, SIFT operator establishes the multi-scale space of image, and Gauss pyramid image is formed by continuous filtering with the different scale Gaussian kernel functions and down samplings. And then the multi-scale DOG (difference-of-Gaussian) space is acquired by subtracting two adjacent scale Gaussian images. Moreover, each point is compared with adjacent scale point and adjacent position point in DOG scale space, the local extreme position, namely the position of feature point and the corresponding scale, is obtained accordingly. Finally, curve fitting is used to accurately locate the feature point, and some points with lower contrast and edge points are deleted. Feature point extraction process of SIFT algorithm is illustrated in Fig. 3.

In this study, the threshold is used to control the amount of feature points extracted by SIFT algorithm. Through experimental testing, the extraction amount of feature points is suitable when the threshold is about 0.65, which can satisfy the requirement of multipoint measurement in civil engineering. The nearest-neighbor algorithm (Beis and Lowe, 1997) is applied to match the feature points extracted by SIFT algorithm. The Euclidean distance of each feature point's descriptor is calculated. Two feature points with the shortest Euclidean distance is regarded as

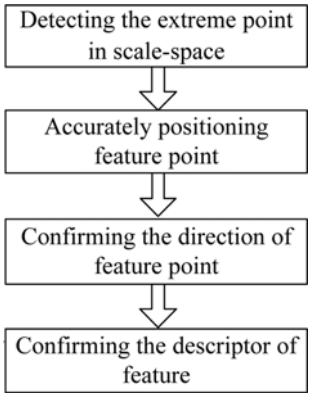

Fig. 3. Feature Point Extraction Process of SIFT Algorithm

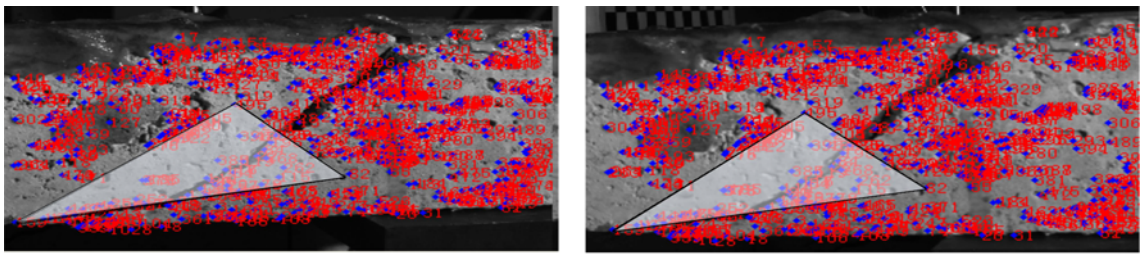

(a) (b)

Fig. 4. Establishment of Structural Plane Equation: (a) Left Image, (b) Right Image

the matching point. To improve matching precision, both limit constraint and uniqueness constraint are used to delete point pairs which can't satisfy these two constraints.

As shown in Fig. 4, blue points on the left and right crack images are expressed by the same number, are the feature points extracted by SIFT algorithm. The aim is to establish the equation of structural plan where cracks are located under the left camera coordinate system by selecting any three points, which do not line up.

As can be seen from Fig. 4, the feature points extracted by SIFT algorithm can't be ensured to lie exactly on the crack edge. As a result, Eq. (1) can't be directly used to calculate the 3D coordinates of crack edge. 3D coordinates of crack edge must be achieved by the process described in section 2. It should be noted that only the crack image captured by the left camera is utilized to extract the crack edge during this process. This isn't be involved the matching problem with the crack image captured by the right camera.

3.2 Extraction of Crack Edge

Firstly, this paper employs the traditional edge extraction method to achieve pixel location of crack edge. There exist some traditional edge extraction methods such as Roberts operator (1963), Sobel operator (1970), Log operator (Marr and Hildreth, 1980), and Canny operator (1986). Compared with other operators, Canny operator has the advantages of simple operation, fast processing speed, noise interference resistance and weak edge detection. Therefore, this study select Canny operator to locate crack edge coarsely.

Traditional Canny algorithm adopts Gaussian filter to smooth image. The amplitude and direction of gray grad are calculated with window. And then gradient image is processed with non-maximum suppression. Finally, the double threshold method is adopted to detect and connect edge. However, there no exists the unified standard for choosing two thresholds, which are usually set artificially. Under the effect of shooting and illumination, edge detection results obtained by traditional Canny operator is usually different from that one under ideal condition for the same image. Moreover, the threshold will be different according to grey distribution range of corresponding image.

To address this issue, this paper processes crack edge further on the base of Canny operator algorithm. The subpixel edge detection method based on Zernike orthornomal moment is introduced (Ghosal, 1993). Zernike orthornomal moment has the advantages of rotation invariance, small information redundancy and high location precise. According to rotation invariance of Zernike orthornomal, Zernike orthornomal algorithm calculates four edge parameters. Four parameters used for edge detection are the background gray h, the step gray k, the distance between the center and edge l, the angle between vertical line of edge and x axis φ, respectively.

Among four parameters of edge point, only l and φ are used to implement Zernike algorithm. As a result, only two masks, namely A_{11} and A_{20}, are required to deduce. Masks of A_{11} and A_{20} are shown in Fig. 5 and 6, respectively, the detailed derivation process refers to the reference (Qu and Cui, 2005). The convolution between the models and 7 × 7 neighbor grey value of pixel point is executed during calculation. The rotation angle φ and l of the edge point are obtained accordingly. Finally, the subpixel coordinate of edge point is given as follows:

$$\begin{vmatrix} x' \\ y' \end{vmatrix} = \begin{vmatrix} x \\ y \end{vmatrix} + l \begin{vmatrix} \cos\varphi \\ \sin\varphi \end{vmatrix} \tag{6}$$

0.000	0.015	0.019	0.000	-0.019	-0.015	0.000
0.022	0.047	0.023	0.000	-0.023	-0.047	-0.022
0.057	0.047	0.023	0.000	-0.023	-0.047	-0.057
0.070	0.047	0.023	0.000	-0.023	-0.047	-0.070
0.057	0.047	0.023	0.000	-0.023	-0.047	-0.057
0.022	0.047	0.023	0.000	-0.023	-0.047	-0.022
0.000	0.015	0.019	0.000	-0.019	-0.015	0.000

(a)

0.000	-0.022	-0.022	-0.022	-0.022	-0.022	0.000
-0.015	-0.047	-0.047	-0.047	-0.047	-0.047	-0.015
-0.019	-0.023	-0.023	-0.023	-0.023	-0.023	-0.019
0.000	0.000	0.000	0.000	0.000	0.000	0.000
0.019	0.023	0.023	0.023	0.023	0.023	0.019
0.015	0.047	0.047	0.047	0.047	0.047	0.015
0.000	0.022	0.022	0.022	0.022	0.022	0.000

(b)

Fig. 5. Mask of A_{11}: (a) Real Component, (b) Imaginary Component

0.000	0.023	0.039	0.041	0.039	0.023	0.000
0.023	0.027	-0.013	-0.026	-0.013	0.027	0.023
0.039	-0.013	-0.053	-0.066	-0.053	-0.013	0.039
0.041	-0.026	-0.066	-0.081	-0.066	-0.026	0.041
0.039	-0.013	-0.053	-0.066	-0.053	-0.013	0.039
0.023	0.027	-0.013	-0.026	-0.013	0.027	0.023
0.000	0.023	0.039	0.041	0.039	0.023	0.000

Fig. 6. Mask of A_{20}

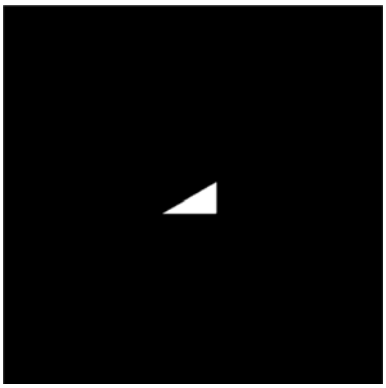

Fig. 7. Triangle Gray Image

where (x', y') is subpixel coordinate of edge point, (x, y) is pixel coordinate of edge point.

Aiming at the precision problem that Canny algorithm only obtain pixel edge, this paper finally presents a Canny-Zernike combination algorithm to achieve subpixel crack edge. This proposed algorithm adopts the edge point inspection and connection method based on the gradient direction. It can reduce noise very well and protect edge details as far as possible, thus better solving the above problem about Canny algorithm. This proposed combination algorithm further improves the performance of Canny algorithm, and acquire subpixel precision location of crack edge detection.

To validate efficiency and detection accuracy of the proposed algorithm, a binary image with a pixel resolution of 1000×1000 is generated by MATLAB. As shown in Fig. 7, a right triangle is put on the center of image, the angle between the hypotenuse and vertical leg is 60°. The gray value of the triangle area is 1, and the grey value of background is 0. The vertical leg of the triangle is located at rows 467-548 and column 559 of the image matrix. The base of the right triangle is positioned at row 548 and cloumns 418-559 of the image matrix. The proposed algorithm is used to execute subpixel edge detection on three sides of the right triangle in image. Subpixel coordinates of the base, vertical leg and hypotenuse are all obtained according to Eq. (6), they are compared with the corresponding actual coordinates. The detection results are shown in Tables 1-3.

Table 1. Subpixel Coordinate Detection of Base (pixel)

No.	Actual coordinates	Canny-Zernike algorithm coordinates	Error
1	(548.5, 490)	(548.4873, 490)	0.0127
2	(548.5, 491)	(548.4873, 491)	0.0127
3	(548.5, 492)	(548.4873, 492)	0.0127
4	(548.5, 493)	(548.4873, 493)	0.0127
5	(548.5, 494)	(548.4873, 494)	0.0127
6	(548.5, 495)	(548.4873, 495)	0.0127
7	(548.5, 496)	(548.4873, 496)	0.0127
8	(548.5, 497)	(548.4873, 497)	0.0127
9	(548.5, 498)	(548.4873, 498)	0.0127
10	(548.5, 499)	(548.4873, 499)	0.0127

Table 2. Subpixel Coordinate Detection of Vertical Leg (pixel)

No.	Actual coordinates	Canny-Zernike algorithm coordinates	Error
1	(500, 559.5)	(500, 559.4798)	0.0202
2	(501, 559.5)	(501, 559.4798)	0.0202
3	(502, 559.5)	(502, 559. 4798)	0.0202
4	(503, 559.5)	(503, 559. 4798)	0.0202
5	(504, 559.5)	(504, 559. 4798)	0.0202
6	(505, 559.5)	(505, 559. 4798)	0.0202
7	(506, 559.5)	(506, 559. 4798)	0.0202
8	(507, 559.5)	(507, 559. 4798)	0.0202
9	(508, 559.5)	(508, 559. 4798)	0.0202
10	(509, 559.5)	(509, 559. 4798)	0.0202

Table 3. Subpixel Coordinate Detection of Hypotenuse (pixel)

No.	Actual coordinates	Canny-Zernike algorithm coordinates	Error
1	(533.5, 442)	(533.4857, 442)	0.0143
2	(531.5, 445)	(531.4763, 445)	0.0237
3	(530.5, 447)	(530.4715, 447)	0.0285
4	(529.5, 449)	(529.4857, 449)	0.0143
5	(527.5, 552)	(527.4763, 552)	0.0237
6	(526.5, 454)	(526.4715, 454)	0.0285
7	(525.5, 456)	(525.4857, 456)	0.0143
8	(523.5, 459)	(523.4763, 459)	0.0237
9	(522.5, 461)	(522.4857, 461)	0.0143
10	(520.5, 464)	(520.4763, 464)	0.0237

As can be seen from Tables 1-3, the accuracy of subpixel edge detection of the base is 0.0127 pixel. The accuracy of subpixel edge detection of the vertcial leg is 0.0202. The accuracy of subpixel edge detection of the hypotenuse is 0.0209 pixel. Experimental results indicate that the Canny-Zernike combination algorithm can achieve the precision of 0.02 pixel when it is used to extract subpixel edge.

In this study, MATLAB is chosen to accomplish the proposed method. Crack width curve is acquired by processing of the left and right crack image. The detailed flowchart of crack width measurement is shown in Fig. 8. The extraction process of crack edge is illustrated in Fig. 9. The measurement process of crack width is described as follows:

(i) Establishing the space plane equation of concrete surface

This study employs SIFT algorithm and the nearest neighbor algorithm to perform feature extraction and matching on the left and right crack image. Any three feature points, which do not line up, are chosen to establish the space plane equation of

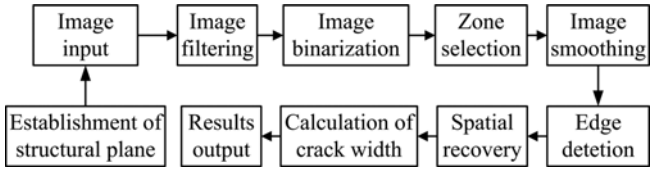

Fig. 8. Flowchart of Crack Width Evaluation Approach

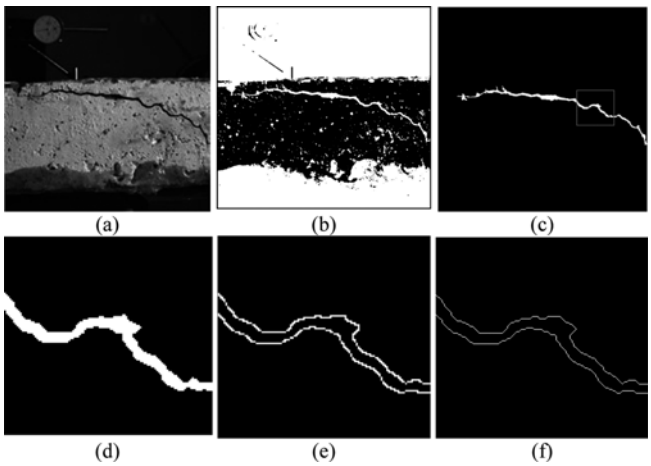

Fig. 9. Process of Crack Edge Extraction: (a) Original Image, (b) Binary Image, (c) Crack Extraction, (d) Selection of Inspection Zone, (e) Canny Extraction, (f) Canny-Zernike Extraction

concrete surface where cracks are positioned according to Eqs. (4) and Eq. (5).

(ii) Image preprocessing

Both self-adaptive histogram and the median filtering are adopted to enhance the contrast ration, remove noise, and protect feature of crack edge.

(iii) Image binarization

The Otsu method (Otsu, 1979; Gong *et al.*, 1998) is utilized to set the gray threshold according to the feature that the gray value of crack area is less than that of background. Therefore, the crack can be extracted from the crack image by segmenting the foreground image from the background image.

(iv) Selection of inspection zone

Cracks on concrete surface are usually ranging up to several millimeters in length, thus measuring crack width within the whole length range makes no sense. To reduce workload, the inspection zone should be preliminarily confirmed in the definite measurement range.

(v) Image Smoothing

To remove burr of crack edge, the mathematical morphology method is used to remove the isolated small zone of the binary image processed by above steps. The crack edge is smoothed by the morphological dilation for realizing the following precise edge detection.

(vi) Edge Detection

A novel Canny-Zernike combination algorithm is employed to obtain the image coordinates of crack edge. Canny algorithm is roughly located the crack edge of preprocessed left image, and then Zernike operator template completes convolution on the pixel edge to achieve the subpixel image coordinates of crack edge. This proposed combination algorithm improves the performance of Canny algorithm, fully plays respective advantages of two algorithms, and remarkably increases the location precise.

(vii) Image coordinates of crack edge on the normalized virtual imaging plane

Equation (3) is used to calculate image coordinates of crack edge curve on the normalized virtual imaging plane.

(viii) Recovering 3D coordinates of crack edge on the space plane

As shown in Fig. 2, the 3D coordinates of crack edge on structural plane are recovered by calculating the intersection coordinates between the straight line op' and the space plane where cracks are located.

(ix) Crack Width calculation

According to Eq. (2), the crack width can be gained and displayed in curve form.

4. Experiments of Crack Width Detection

4.1 Experimental Setup

As shown in Fig. 10, the integrated stereovision measurement system comprises a computer, two CCD cameras, a tripod, and the crack width measurement software. The cameras come with a 2/3 inch CCD and could record high-definition images with a pixel resolution of 1000 × 1000 at 40 fps. They are equipped with an optical zoom lens of F1.8-16 and focal length ranging between 12-30 mm. In this work, the manufactured camera tripod can adjust horizontal distance, pitch angle and horizontal angle to satisfy the stereovision detection demand.

On the base of the above algorithms, the crack width detection software is developed and is integrated into the stereovision measurement system with hardware. The software is an independent executive procedure, including two modules of image capturing and image processing, has the functions of image sampling, displaying, saving, analyzing and results output.

4.2 Experimental Setting

Three concrete beams with surface cracks, generated in the destructive static load test, were used to inspect crack widths. The cross-sections of each concrete beams was 70 mm × 90 mm in the test, and the length was 900 mm. An 8-mm-diameter BFRP bar was contained in each concrete beam. The concrete grade is C30, and the thickness of concrete cover was 31 mm.

In the experiment, the stereovision measurement system was placed 0.5 m away from the concrete beam, and the fields of cameras were both about 180 mm × 180 mm. A 1300w halogen tungsten lamp worked with the aperture to adjust exposure.

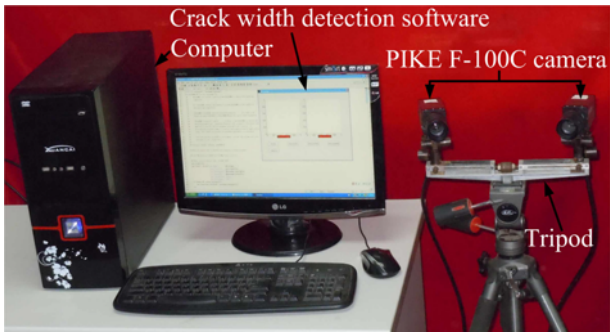

Fig. 10. Stereovision Measurement System

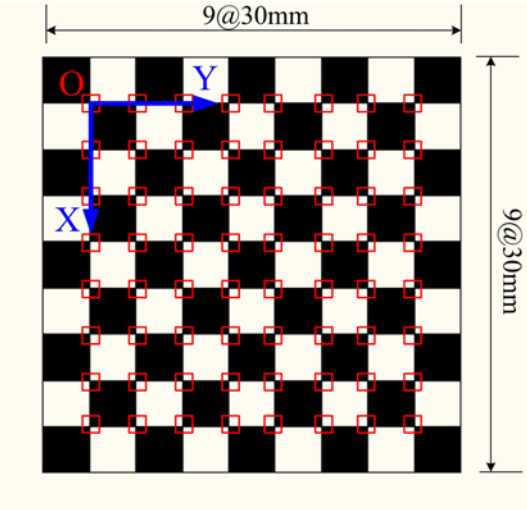

Fig. 11. Planar Pattern

During the test, the stereovision measurement system was firstly calibrated by the plane pattern as shown in Fig. 11. The plane pattern consisted of eighty-one 30 mm × 30 mm black and white squares. The image coordinate of each corner point of 2D planar pattern was extracted through Hough transforming algorithm (Illingworth, 1988), and the actual 3D coordinates of each corner point was accordingly assigned. 9 images of the planar pattern in different postures were separately captured by the left and right cameras. According to Zhang's calibration algorithm, the intrinsic and extrinsic parameters including nonlinear distortion factors of stereovision measurement system were all obtained.

Then, the crack images of each concrete beam were captured by the integrated system. It should be noted that surface cracks of concrete beams should be at the center of field-of-view. Finally, the synchronized crack images were processed by the crack width inspection software, and the crack width curves were acquired at the given positions. At the same time, the crack width gauge with 0.02 mm precision was also utilized to measure the crack widths at the corresponding position for comparison of two methods' inspection results.

4.3 Experimental Results

To verify the proposed crack width detection approach in this paper, two inspection zones of each beam were chosen to measure crack width. Five positions of each inspection zone were selected to compare the measurement results of the crack width gauge and the proposed method.

The inspection results of specimen 1 are shown in Fig. 12. Five positions of each zone were also measured by the crack width gauge, and the corresponding results were listed in Tables 4 and 5, respectively. As can be seen from Tables 4 and 5, the maximum error is 0.046 mm and the maximum relative error is 4.0% towards crack width within 1 mm. The reason that the error of zone-2 detection results is larger than that of zone-1 is that the crack edge of zone-2 is jagged. This affects the extraction precision

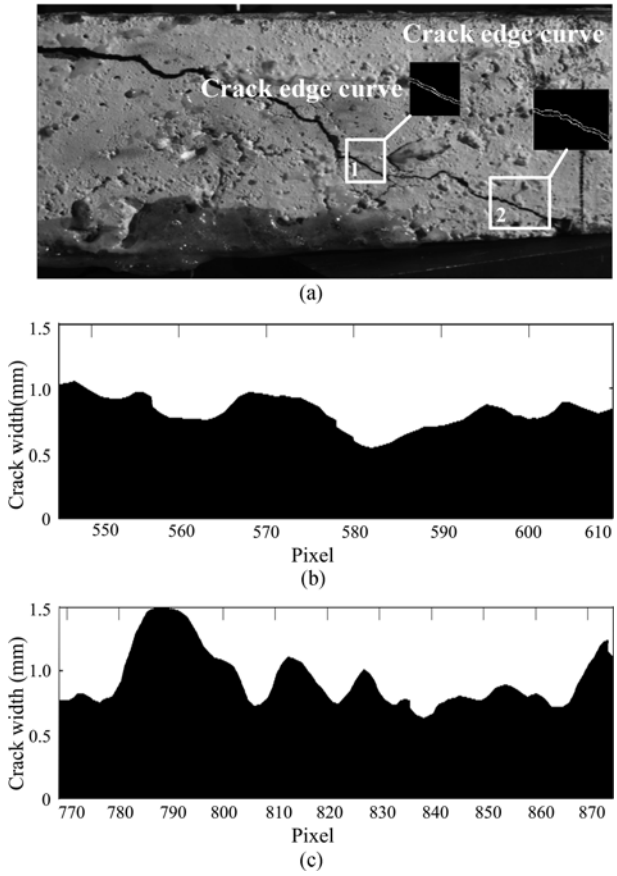

Fig. 12. Crack Width Inspection Results of Specimen 1: (a) Inspection Zone of Crack, (b) Crack Width Curve of Zone-1, (c) Crack Width Curve of Zone-2

Table 4. Zone-1 Crack Width Comparison of Specimen 1

Detection method (mm)	P-1	P-2	P-3	P-4	P-5
Crack width gauge	0.960	0.720	0.520	0.840	0.600
Stereovision	0.969	0.746	0.536	0.873	0.576
Error	0.009	0.026	0.016	0.033	-0.024
Relative error	0.9%	3.7%	3.1%	3.9%	-4.0%

Table 5. Zone-2 Crack Width Comparison of Specimen 1

Detection method (mm)	P-1	P-2	P-3	P-4	P-5
Crack width gauge	0.760	1.440	0.680	0.640	1.160
Stereovision	0.764	1.486	0.701	0.626	1.180
Error	0.004	0.046	0.021	-0.014	0.020
Relative error	0.5%	3.2%	3.1%	-2.2%	1.7%

of crack edge. To address this issue, the crack extraction algorithm should be improved.

The surface cracks measurement results of specimen 2 are illustrated in Fig. 13, Tables 6 and 7, respectively. The comparison results measured by two methods demonstrate that the maximum error is 0.061 mm and the maximum relative error is 5.4% towards cracks width between 1-2 mm. The reason that the error

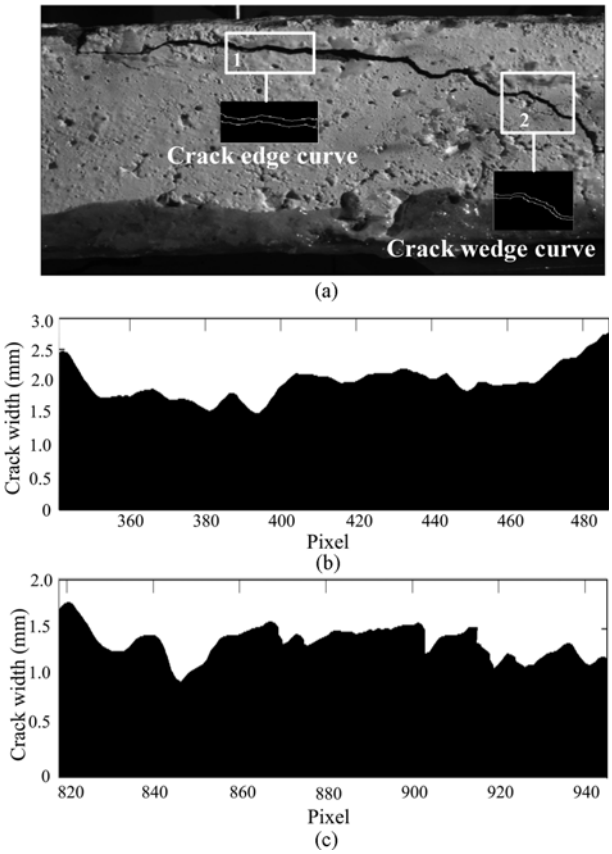

Fig. 13. Crack Width Inspection Results of Specimen 2: (a) Inspection Zone of Crack, (b) Crack Width Curve of Zone-1, (c) Crack Width Curve of Zone-2

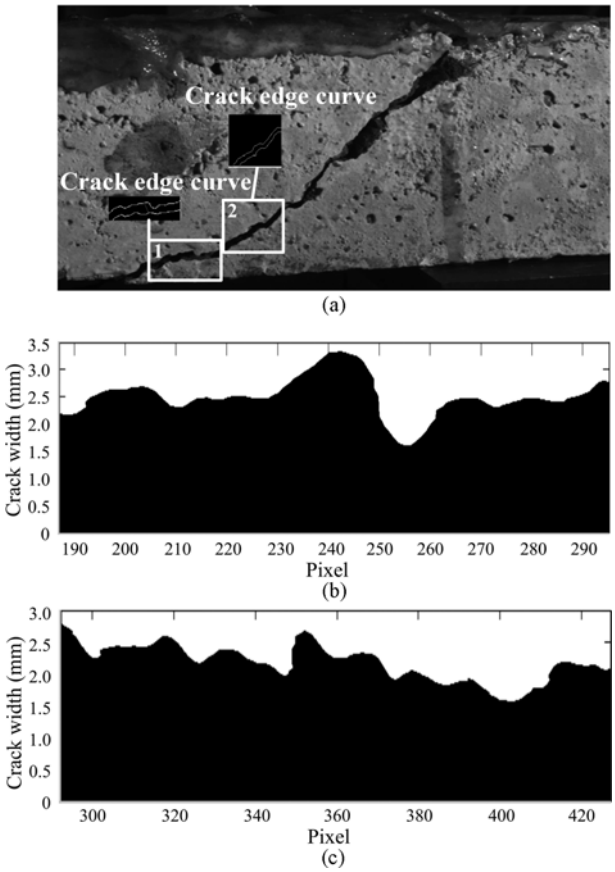

Fig. 14. Crack Width Inspection Results of Specimen 3: (a) Inspection Zone of Crack, (b) Crack Width Curve of Zone-1, (c) Crack Width Curve of Zone-2

Table 6. Zone-1 Crack Width Comparison of Specimen 2

Detection method (mm)	P-1	P-2	P-3	P-4	P-5
Crack width gauge	1.680	1.760	1.440	1.940	1.800
Stereovision	1.746	1.810	1.506	2.000	1.843
Error	0.054	0.044	0.056	0.060	0.043
Relative error	3.2%	2.5%	3.9%	3.1%	2.4%

Table 7. Zone-2 Crack Width Comparison of Specimen 2

Detection method (mm)	P-1	P-2	P-3	P-4	P-5
Crack width gauge	1.240	1.420	1.120	1.520	1.360
Stereovision	1.262	1.423	0.959	1.555	1.345
Error	0.042	0.003	-0.061	0.035	-0.015
Relative error	3.4%	0.2%	-5.4%	2.3%	-1.1%

Table 8. Zone-1 Crack Width Comparison of Specimen 3

Detection method (mm)	P-1	P-2	P-3	P-4	P-5
Vernier caliper	2.140	2.26	3.340	1.560	2.440
Stereovision	2.162	2.286	3.319	1.584	2.463
Error	0.022	0.026	-0.021	0.024	0.023
Relative error	1.0%	1.2%	-0.6%	1.5%	0.9%

Table 9. Zone-2 Crack Width Comparison of Specimen 3

Detection method (mm)	P-1	P-2	P-3	P-4	P-5
Vernier caliper	2.720	2.380	2.600	1.880	1.480
Stereovision	2.736	2.408	2.656	1.897	1.500
Error	0.016	0.028	0.056	0.017	0.020
Relative error	0.6%	1.2%	2.1%	0.9%	1.4%

of specimen 2 is bigger than that of specimen 1 is due to the light of some crack areas. This makes the corresponding gray value is either larger or smaller than that of other areas in image, thus affecting the accuracy of crack segmentation during the process of image binarization. As a result, the crack segmentation algorithm needs to set an appropriate threshold used for image binarization.

Figure 14 shows the two zones inspection results of specimen 3 measured by the stereovision method. The maximum range of crack width gauge was only 2 mm. However, some crack width of specimen 3 was larger than 2 mm, so the real value of specimen 3 was detected by the vernier caliper with 0.02 mm precision. The comparison results of two approaches are given in Tables 8 and 9. The experimental results indicate that

the maximum error is 0.056 mm and the maximum relative error is 2.1% towards cracks whose width is greater than 2 mm. The relative error of specimen 3 is less than those of the previous two specimens. The reason lies in that the crack edge is relative clear towards the wider crack, which leads to extract crack edge easily.

5. Conclusions

Contrasting with the traditional visual inspection method with one camera, this paper presents a stereovision-based crack width detection approach. This method does not require to attach a scale to concrete surface for converting measurement units. 3D coordinates of crack edge are recovered through projecting crack on the space plane. Crack edge is extracted by a novel Canny-Zernike combination algorithm which achieves 0.02 subpixel coordinate location. The crack width is quantitatively evaluated by the minimum distance between two sides of crack edge. Two zone's surface cracks on each concrete beam are measured by the proposed technique. Experimental results demonstrate that the proposed stereovision-based crack width approach has a higher precision, verifying that the proposed method is feasible and useful.

It should be noted that although the accuracy of 2D image measurement method with single-camera is lower than that of 3D measurement, the existing single-camera detection method can basiclly satisfy engineering requirement. In addition, as can be seen from experiments, the stereovision-based crack detection technique is disturbed by ambient light during the test. This affects the extraction precision of crack edge. To increase measurement precision, as part of future work, the crack edge extraction algorithm should be improved, and the threshold which segments crack from background in binary image should be set accurately to recognize the jagged crack. Furthermore, the use of appropriate light source could improve the measurement accuracy of the proposed approach. As part of future work, the effect of lighting conditions on the accuracy of the proposed stereovision method needs to be deeply investigated.

Acknowledgments

This study was supported by the National Natural Science Foundation of China under Grant No. 51478148 and No. 51408165, the Natural Science Foundation of Heilongjiang under Grant No. E201434 and the fundamental research funds for the central universities under Grant no. HIT. NSRIF. 2014104.

References

Beis, J. S. and Lowe, D. G. (1997). "Shape indexing using approximate Nearest-Neighbour search in high-dimensional spaces." *Computer Vision and Pattern Recognition, Proceedings of IEEE Computer Society Conference on*, pp. 1000-1006, DOI: 10.1109/CVPR.1997.609451.

Bellavia, F., Tegolo, D., and Valenti, C. (2011). "Improving harris corner selection strategy." *IET Computer Vision*, Vol. 5, No. 2, pp. 87-96, DOI: 10.1049/iet-cvi.2009.0127.

Canny, J. (1986). "A computational approach to edge detection." *IEEE Transaction on. Pattern Analysis Machine Intelligence*, Vol. 8, No. 6, pp. 679-698, DOI: 10.1109/TPAMI.1986.4767851.

Dare, P., Hanley, H., Fraser, C., Riedel, B., and Niemeier, W. (2003). "An operational application of automatic feature extraction: The measurement of cracks in concrete structures." *The Photogrammetric Record*, Vol. 17, No. 99, pp. 453-464, DOI: 10.1111/0031-868X.00198.

Ghosal, S. and Mehrotra, R. (1993). "Orthogonal moment operators for subpixel edge detection." *Pattern Recognition*, Vol. 26, No. 2, pp. 295-306, DOI: 10.1016/0031-3203(93)90038-X.

Gong, J., Li, L. Y., and Chen, W. (1998). "Fast recursive algorithms for two-dimensional thresholding." *Pattern Recognition*, Vol. 31, No. 3, pp. 295-300, DOI: 10.1016/S0031-3203(97)00043-5.

Illingworth, J. and Kittler, J. (1988). "A survey of the hough transform." *Computer Vision, Graphics, and Image Processing*, Vol. 44, No. 1, pp. 87-116, DOI: 10.1016/S0734-189X(88)80033-1.

Jahanshahi, M. R. and Masri, S. F. (2013). "A new methodology for non-contact accurate crack width measurement through photogrammetry for automated structural safety evaluation." *Smart Materials and Structures*, Vol. 22, No. 3, pp. 035019, DOI: 10.1088/0964-1726/22/3/035019.

Kai, T. W. and Christopher, K. Y. Leung (2007). "Applications of a distributed fiber optic crack sensor for concrete structures." *Sensors and Actuators A: Physical*, Vol. 135, No. 12, pp. 458-464, DOI: 10.1016/j.sna.2006.09.004.

Li, G., Xiao, X. P., and Gui, Y. F. (2009). "A novel algorithm of image denoising based on the grey absolute relational analysis." IEEE International Conference on Grey System and Intelligent Services, Nanjing, China, Vol. 1, pp. 181-185, DOI: 10.1109/GSIS. 2009.5408327.

Li, X. D., Xie, H. M., Kang, Y. L., and Wu, X. P. (2010). "A brief review and prospect of experimental solid mechanics in China." *Acta Mechanica Solida Sinica*, Vol. 23, No. 6, pp. 498-548, DOI: 10.1016/S0894-9166(11)60003-7.

Longuet-Higgins, H. (1981). "A computer algorithm for reconstructing a scene from two projections." *Nature*, Vol. 239, pp. 133-135, DOI: 10.1038/293133a0.

Lowe, D. G. (1999). "Object recognition from local scale-invariant features." *Computer Vision (ICCV), Proceeding of Seventh IEEE International Conference on*, Vol. 2, pp. 1150-1157, DOI: 10.1109/ICCV. 1999. 790410.

Lowe, D. G. (2004). "Distinctive image features from scale-invariant keypoints." *Computer Vision (ICCV), Proceeding of IEEE International Conference on*, Vol. 60, No. 2, pp. 91-110, DOI:10.1023/B: VISI. 0000029664. 99615.94.

Marr, D. and Hildreth, E. (1980). "Theory of edge detection." *Proc. Royal Soc. London B*, Vol. 207, No. 1167, pp. 187-217, DOI: 10.1098/rspb.1980.0020.

McCann, D. and Forde, M. (2001). "Review of NDT methods in the assessment of concrete and masonry structures." *NDT & E International*, Vol. 34, No. 2, pp. 71-84, DOI: 10.1016/S0963-8695(00)00032-3.

Otsu, N. (1979). "A threshold selection method from gray-level histogram." *IEEE Transactions on System, Man, Cybernetics*, Vol. 9, No. 1, pp. 62-66, DOI: 0018-9472/79/0100-0062.

Qu, Y. D. and Cui, C. S. (2005). "A fast subpixel edge detection method using Sobel-Zernike moments operator." *Image and Vision Computing*, Vol. 23, No. 1, pp. 11-17, DOI: 10.1016/j.imavi s.2004.07.003.

Roberts, L. G. (1963). *Machine perception of three dimension solids, Massachusetts Institute of Technology*, PhD Thesis, http://hdl.handle.net/1721.1/11589.

Smith, S. M. and Brady, J. M. (1997). "SUSAN-a new approach to low level image processing." *International Journal of Computer Vision*, Vol. 23, No. 1, pp. 45-78, DOI: 10.1023/A:1007963824710.

Sobel, L. (1970). *Camera models and machine perception*, PhD Thesis, Stanford University, Stanford, CA. USA

Yamaguchi, T. and Hashimoto, S. (2010). "Fast crack detection method for large-size concrete surface images using percolation-based image processing." *Machine Vision and Applications*, Vol. 21, pp. 797-809, DOI: 10.1007/s00138-009-0189-8.

Zhang, W. T., Dai, J. Y., Xu, H., Sun, B. C., and Du, Y. L. (2007). "Distributed fiber optic crack sensor for concrete structures." *Proc. of SPIE, Sandiego*, USA, Vol. 6830, pp. 68300F, DOI: 10.1117/12.757864.

Zhang, Z. Y. (2000). "A flexible new technique for camera calibration." *IEEE Transactions on. Pattern Analysis Machine Intelligence*, Vol. 22, No. 11, pp. 1330-34, DOI: 10.1109/34.888718.